The benefits of Duffing-type nonlinearities and electrical optimisation of a mono-stable energy harvester under white Gaussian excitations

P L Green[a,1], K Worden[a], K Atallah[b], N D Sims[a]

[a] *Department of Mechanical Engineering, University of Sheffield, Mappin Street, Sheffield, United Kingdom, S1 3JD*
[b] *Department of Electrical Engineering, University of Sheffield, Mappin Street, Sheffield, United Kingdom, S1 3JD*

Abstract

This work is concerned with the performance of a single degree of freedom electromagnetic energy harvester when subjected to a broadband white noise base acceleration. Firstly, using the Fokker-Planck-Kolmogorov equation, it is shown that Duffing-type nonlinearities can be used to reduce the size of energy harvesting devices without affecting their power output. This is then verified using the technique of Equivalent Linearisation. Secondly, it is shown analytically that the optimum load resistance of the device is different to that which is dictated by the principle of impedance matching. This result is then verified experimentally.

Key Words: Energy harvesting, Duffing, random excitation, nonlinear vibration, electromagnetic

1. Introduction

In recent years much attention has been focused on the development of microelectromechanical systems (MEMS) which do not have to rely on external energy sources. The advantages of small self-powered sensors are numerous, especially when one considers large systems of sensors such as those that are often used in structural health monitoring applications. In such cases, alleviating the need for an external energy source would eliminate the need for batteries which are often bulky and have a finite shelf-life. Additionally, it may allow sensors to be placed in more hostile or inaccessible environments (such as inside rotating machinery or on bridges). To this end, the concept of harvesting electrical energy from mechanical vibrations has become a popular area of research.

With this aim in mind, a range of different energy harvesting devices have been developed for both MEMS-scale and larger-scale systems. A review of such devices can be found in [1]. In one of the earliest studies [2], an energy harvesting device was proposed which relied on the electromagnetic induction that can be observed in a coil of wire when it is placed in a time varying magnetic flux (Faraday's law). To achieve this, a permanent magnet was attached to a vibrating base such that, when excited, the magnet oscillated within the coil. The device was modelled as a base excited mass-spring-damper where the damper was used to

URL: mep09plg@shef.ac.uk (P L Green)

represent a combination of parasitic losses and the transfer of energy from the mechanical to the electrical domains. Subsequently, the dynamic response and power output of other linear single-degree-of-freedom (SDOF) system devices to harmonic base excitations were analysed in several works (for example, [3], [4], [5] and [6]).

In [3] it was concluded that such an energy harvesting device will produce the most power if the damping caused by the electromagnetic coupling was equal to the mechanical damping present in the system, but that such a large coupling may be difficult to obtain. A detailed analysis of the ability of such devices to deliver power across a load resistor was also provided in [4]. It was concluded that maximum power output could be achieved when the coil resistance was equal to the damping that was introduced by the combination of mechanical and electrical losses in the device. While many of the afore mentioned works focused on the response of energy harvesting devices to sinusoidal excitations, it was soon realised that many ambient vibrations sources can actually be somewhat stochastic in nature. This led to a significant body of work which focused on analysising the response of energy harvesters to random excitations ([7, 8, 9, 10, 11]) - something which will also be the focus of this paper.

With regards to the parasitic damping present in such a device it is intuitive to suggest that the minimisation of mechanical losses will maximise the energy available for transfer into the electrical domain. However, in [5] it was pointed out that a reduction in mechanical damping will lead to higher amplitude oscillations which may not be possible in small devices. As a result, it was concluded that size is one of the main limiting factors with respect to energy harvester design - especially when considering devices which are designed to work alongside microelectromechanical systems.

Another conclusion that can be drawn from the literature is that the device proposed in [2] would only produce useful amounts of power if excited close to its resonance frequency and will therefore only perform well over a narrow bandwidth. As the dominant frequencies of most ambient vibrations are broadband or time dependent one can hypothesise that such a device will need to operate well over a larger bandwidth if it is to be used in many real world applications (the characteristics of several different types of ambient vibration are described in [12]).

Consequently, much effort has been directed towards the development of devices which are designed to work well over a larger bandwidth (reviews of which can be found in [13] and [14]). Of particular interest here is the findings shown in [15] where it was suggested that the introduction of Duffing-type nonlinearities into an SDOF electromagnetic device may help to extend its useful bandwidth. To achieve this, the centre magnet of the device was held in suspension by two outer magnets which were orientated such that their poles were repelling that of the centre magnet. It was shown that this introduced a cubic spring term, similar to that

of the mono-stable hardening spring Duffing oscillator. This nonlinearity had the effect of 'skewing' the frequency response of the device which, it was hypothesised, may allow the device to function well over a larger bandwidth. Subsequently in [9] the response of the device to a broadband white noise excitation was analysed using the Fokker-Planck-Kolmogorov (FPK) equation. It was concluded that the nonlinear stiffness term had no effect on the velocity probability density function of the centre magnet and, as a result, had no benefit with regards to power output. This was subsequently confirmed using experimentally validated simulations in [16].

In this paper, the response of a mono-stable device with Duffing-type nonlinearities is investigated. The effects of inductance are considered negligible thus allowing the device to be modelled as an SDOF system. Its response to broadband white noise accelerations is then analysed using the FPK equation. It is shown that although the induced nonlinearity cannot be used to improve power output, it can be used to reduce the maximum displacement amplitude of the centre magnet without effecting device performance and as a result, can be used to create smaller energy harvesting devices. The method of Equivalent Linearisation is then used to verify this fact. The device is then modelled such that it is generating power across a load resistance. The FPK equation is then used to find the optimum load resistance which will maximise power output. Although the principle of impedance matching [17] states that the optimum load resistance is equal to that of the coil of the device, the analysis in this work shows that, when under the afore-mentioned random excitation conditions, this is not the case. In fact, it is shown that the optimum load resistance becomes a function of the rate of change of magnetic flux present in the device. Experimental tests are then used to verify these findings. The tests also confirm certain commonly used assumptions with respect to the electromagnetic coupling, and show that when modelling real energy harvesting devices the effects of friction may need to be considered.

2. Governing Equations

A schematic of the mechanical component of a SDOF energy harvesting device with a cubic stiffness nonlinearity is shown in Figure 1 (a). Using an electromagnetic coupling to transfer kinetic energy into the electrical domain (Faraday's law) and connecting the device to a load resistance realises the circuit diagram shown in Figure 1 (b).

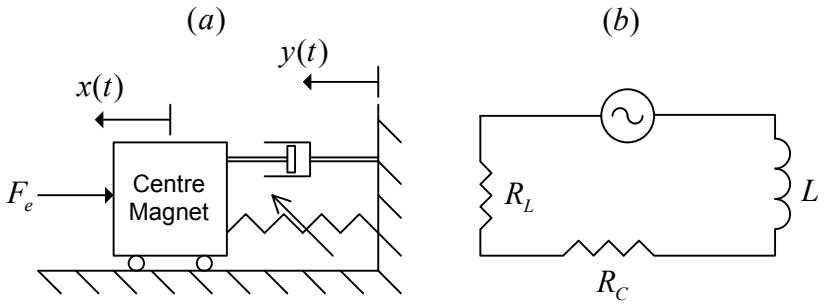

Figure 1: Schematics of (a) mechanical and (b) electrical elements of the device.

2.1. Equation of Motion

The equation of motion of the device in Figure 1 (a) is:

$$m\ddot{z} + c\dot{z} + kz + k_3 z^3 + F_e = -m\ddot{y}, \tag{1}$$

where $z = x - y$, m is the mass of the centre magnet, c is the viscous mechanical damping coefficient, k is the linear stiffness term, k_3 is the nonlinear stiffness term and F_e is the force on the centre magnet due to the electromagnetic coupling. From Faraday's law, one can write:

$$E_{ind} = -\frac{d\Phi}{dt} = -\frac{d\Phi}{dz}\dot{z}, \tag{2}$$

where E_{ind} is the induced electromotive force and Φ is the magnetic flux. Equating the instantaneous power between the mechanical and electrical domains gives:

$$F_e\dot{z} = iE_{ind}, \tag{3}$$

where i is the current flowing within the coil. Combining Equations 2 and 3 one finds that:

$$F_e = -i\frac{d\Phi}{dz}. \tag{4}$$

Applying Kirchoff's voltage law to the circuit in Figure 1 (b) yields:

$$i(R_L + R_C) + L\frac{di}{dt} = -\frac{d\Phi}{dz}\dot{z}, \tag{5}$$

where R_L is load resistance, R_C is coil resistance and L is inductance. For low frequency applications it is assumed that L is negligible so that:

$$F_e = \alpha^2\frac{1}{R_L + R_C}\dot{z}, \tag{6}$$

where $\alpha = \frac{d\Phi}{dz}$. Assuming α is constant over the region of interest, the equation of motion can be written as:

$$\ddot{z} + (2\omega_n\zeta + \gamma/m)\,\dot{z} + \omega_n^2 z + \beta z^3 = -\ddot{y}, \tag{7}$$

where ζ is the damping ratio, ω_n is the natural frequency, $\beta = k_3/m$ and $\gamma = \frac{\alpha^2}{(R_L+R_C)}$. One can see that, using this model, the effect of the electromagnetic coupling is modelled as an extra viscous damping term, γ.

2.2. Power through Load Resistor

Electrical power can be calculated from the instantaneous power given in equation (3):

$$iE_{ind} = F_e\dot{z} = \frac{\alpha^2\dot{z}^2}{R_L + R_C} = \frac{R_L\alpha^2 z_2^2}{(R_L + R_C)^2} + \frac{R_C\alpha^2 z_2^2}{(R_L + R_C)^2}, \tag{8}$$

such that the power delivered to the load is given by:

$$P_{load} = \frac{R_L\alpha^2\dot{z}^2}{(R_L + R_C)^2} = \frac{R_L\dot{z}^2\gamma}{(R_L + R_C)}. \tag{9}$$

3. Response to a Broadband White Noise Excitation

In this section, the response of the device to broadband white noise base acceleration is analysed[1]. The properties of the excitation signals are as follows:

$$E[\ddot{y}(t)] = 0, \tag{10}$$

$$E[\ddot{y}(t_1)\ddot{y}(t_2)] = \frac{S}{2}\delta(t_1 - t_2), \tag{11}$$

where E represents the expected value, S the white power spectral density, and δ the Dirac delta function. The response of the device is analysed using the Fokker-Planck-Kolmogorov (FPK) equation. For a derivation of the FPK equation and examples of its applications to some dynamic systems, references [18] and [19] are suggested.

Allowing $z_1 = z$ and $z_2 = \dot{z}$ then the FPK equation needed to find the stationary probability density function (PDF) of the device is given by:

$$0 = -\frac{\partial}{\partial z_1}(z_2 p) + \frac{\partial}{\partial z_2}\left(\left(\left(2\omega_n\zeta + \gamma/m\right)z_2 + \omega_n^2 z_1 + \beta z_1^3\right)p\right) + \frac{S}{4}\frac{\partial^2}{\partial z_2^2}p, \tag{12}$$

where p is the joint PDF of the system. This can be written as:

$$0 = \left[-z_2\frac{\partial p}{\partial z_1} + \frac{\partial p}{\partial z_2}(\omega_n^2 z_1 + \beta z_1^3)\right] + \left[\eta p + \eta z_2\frac{\partial p}{\partial z_2} + \frac{S}{4}\frac{\partial^2 p}{\partial z_2^2}\right]. \tag{13}$$

The stationary probability density function of this system can be found to be:

$$p = A_1 e^{-\frac{4(2\omega_n\zeta+\gamma/m)}{S}\left(\frac{\omega_n^2}{2}z_1^2 + \beta z_1^4\right)} \times A_2 e^{-\frac{2(2\omega_n\zeta+\gamma/m)z_2^2}{S}}, \tag{14}$$

[1]The FPK equation was first used to analyse the response of an energy harvester of this type to white gaussian excitations in [9]. The derivation presented here is shown merely for the sake of readability.

(for the sake of completeness, the detailed steps are shown in Appendix A). Upon studying equation (14) one can see that the joint PDF of the system has been expressed in the form:

$$p(z_1, z_2) = p(z_1)p(z_2), \tag{15}$$

where:

$$p(z_1) = A_1 e^{-\frac{4(2\omega_n\zeta+\gamma/m)}{S}\left(\frac{\omega_n^2}{2}z_1^2+\beta z_1^4\right)}, \tag{16}$$

and

$$p(z_2) = A_2 e^{-\frac{2(2\omega_n\zeta+\gamma/m)z_2^2}{S}}. \tag{17}$$

By being able to separate the joint PDF into the form $p(z_1)p(z_2)$ one can conclude that the stationary relative displacement and relative velocity PDFs of the system are independent of each other. Consequently, changing a variable which is present in $p(z_1)$ but not in $p(z_2)$ (β in this case) allows one to alter the relative displacement PDF without effecting that of the relative velocity. This result is important with regards to some of the conclusions drawn in this paper and its significance is discussed further in the following section.

4. Benefits of Duffing-type Nonlinearities

From equation (14) it can be seen that β has no influence on the relative velocity PDF and therefore cannot effect the power output of the device (as stated in [10] and [16]). However, the nonlinearity does affect the relative displacement PDF and can therefore be used to reduce the maximum displacement of the centre magnet without effecting the power output. In [5] the maximum possible amplitude of the centre magnet was identified as one of the limiting factors with respect to device performance and equation (14) shows that the nonlinear spring term is beneficial in this respect.

To quantify the effect of the nonlinearity, the variance of the relative displacement PDF can be found using:

$$\sigma_{z_1}^2 = \int_{-\infty}^{\infty} z_1^2 p_1(z_1)p_2(z_2)dz_1dz_2, \tag{18}$$

the solution of which is beyond the scope of the present work. For the full solution to equation (18) the reader is directed towards reference [20] where the displacement variance is shown to be:

$$\sigma_{z_1}^2 = \sqrt{\frac{S}{8\beta(2\omega_n\zeta+\gamma/m)}}U\left(1, \frac{1}{\sqrt{2\rho}}\right)U\left(0, \frac{1}{\sqrt{2\rho}}\right)^{-1}, \tag{19}$$

where U is the parabolic cylindrical function (as defined in [21]) and

$$\rho = \frac{\beta S}{4\omega_n^4(2\omega_n\zeta+\gamma/m)}. \tag{20}$$

From a design perspective, if the parameters of the device are known then equation (19) can be used to estimate the maximum relative displacement of the centre magnet to within a desired level of confidence for different levels of nonlinearity. Defining the maximum relative displacement of the centre magnet as its value three standard deviations from the mean, Figure 2 shows how the maximum amplitude decreases as the nonlinear spring term is increased.

Following this, the equation of motion of the device was put into state space form so that its response to a white noise input could be analysed numerically using the fourth order Runge-Kutta method. Using this method, Monte-Carlo simulations were run to validate the results according to equation (19). This is shown in Figure 2. It should be noted that, by measuring the relative displacement three standard deviations from the mean one is estimating the maximum possible relative displacement to within a 99.7 % confidence interval.

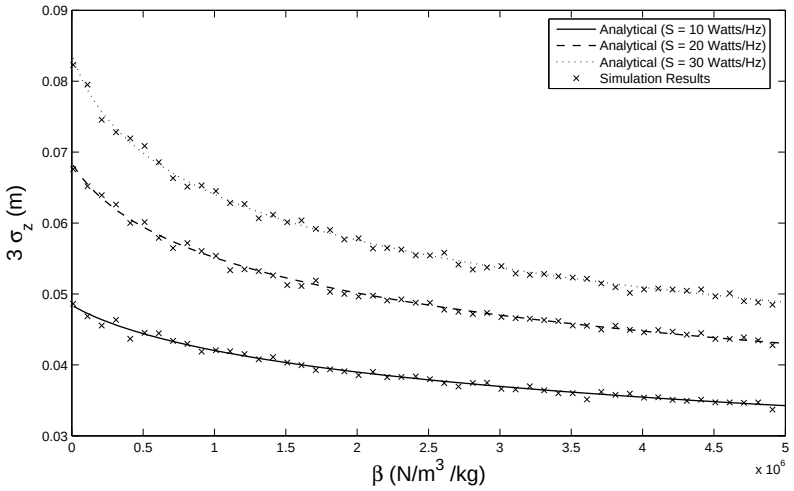

Figure 2: Variation of maximum centre magnet relative displacement amplitude with β, estimated to within a 99.7 % confidence interval where $m = 0.02$ kg, $\alpha = 0.2$ Henry/m, $R_L = 0.5$ Ohms, $R_C = 0.5$ Ohms, $\zeta = 0.05$ $\omega_n = 40$ rad/s and S=10 Watts/Hz. The line and crosses represent analytical (from equation (19)) and simulation results respectively.

4.1. Equivalent Linearisation

Although equation (19) is able to demonstrate the effect of Duffing-type nonlinearities on the relative displacement variance of the device it is not an equation which can be easily interpreted. Consequently, the purpose of this section was to use the technique of Equivalent Linearisation to develop an expression for the relative displacement variance which, although less accurate, is easier to understand and interpret.

Equivalent Linearisation is concerned with the development of a linear system which is able to match the response of a nonlinear system as closely as possible. This then allows the behavior of the nonlinear system to be approximated by analysing the behavior of its equivalent linear counterpart. While appropriate in this case, there is some behavior which is impossible to replicate using an equivalent linear system - the

inter-well dynamics of a bi-stable oscillator for example. The theory of this technique is expanded more in the following dynamics text books ([20] [22]).

Recalling the equation of motion of the device:

$$\ddot{z} + \frac{\theta}{m}\dot{z} + \frac{k}{m}z + \frac{k_3}{m}z^3 + = -\ddot{y}(t), \tag{21}$$

where for simplicity θ represents a combination of electrical and parasitic damping:

$$\theta = c + \frac{\alpha^2}{R_L + R_C}. \tag{22}$$

The purpose of the following analysis is to find a system of the form:

$$\ddot{z} + \frac{\theta}{m}\dot{z} + \frac{k_{eq}}{m}z = -\ddot{y}(t), \tag{23}$$

which can replicate the response of the nonlinear system as accurately as possible. In [22] it is shown that the equivalent stiffness of such a system is given by:

$$k_{eq} = k + \frac{E[f(z)z]}{E[z^2]}, \tag{24}$$

where $f(z)$ is the nonlinear stiffness function to be analysed and

$$E[f(z)z] = \int_{\infty}^{\infty} p\left(f(z)z\right) f(z) z dz. \tag{25}$$

Upon studying equation (25) one can see that in order to evaluate k_{eq} one must know the PDF of the nonlinear system ($p\left(f(z)z\right)$). This is problematic as the PDFs of general nonlinear systems are not known. As a result, the PDF is approximated by that of a linear system, so that one can make use of the fact the a linear system excited with a zero mean gaussian excitation will have a zero mean gaussian response. Using the knowledge that the PDF of the linear system (equation (23)) is:

$$p(z)_{eq} = \frac{1}{\sqrt{2\pi}\sigma_{z(eq)}} e^{-\frac{2k_{eq}z^2\theta}{Sm^2}}, \tag{26}$$

and setting $f(z) = k_3 z^3$ then equation (25) becomes:

$$k_{eq} = k + \frac{k_3}{\sqrt{2\pi}\sigma^3_{z(eq)}} \int_{-\infty}^{\infty} e^{-\frac{2k_{eq}z^2\theta}{Sm^2}} z^4 dz. \tag{27}$$

The relative displacement variance of the equivalent linear system is found from:

$$\sigma^2_{z(eq)} = \int_{\infty}^{\infty} e^{-\frac{2k_{eq}z^2\theta}{Sm^2}} z^2 dz, \tag{28}$$

which leads to:

$$\sigma^2_{z(eq)} = \frac{Sm^2}{4k_{eq}\theta}. \tag{29}$$

Solving equation (27) (the solution to integrals of this type is shown in [22]) and neglecting negative values of k_{eq} one finds that the equivalent linear stiffness is given by:

$$k_{eq} = \frac{1}{2}\frac{\theta k + \sqrt{\theta^2 k^2 + 3k_3 S m^2 \theta}}{\theta}. \tag{30}$$

Having found the equivalent stiffness, equation (29) was used to find the variance of the linear equivalent system. Figure 3 shows the relative displacement variance according of the according to equation (29) compared with that obtained using Monte-Carlo simulations (using the same system properties as was used in Figure 2). It can be seen that the Equivalent Linearisation technique can provide a good estimate of the relative displacement variance as k_3 is altered.

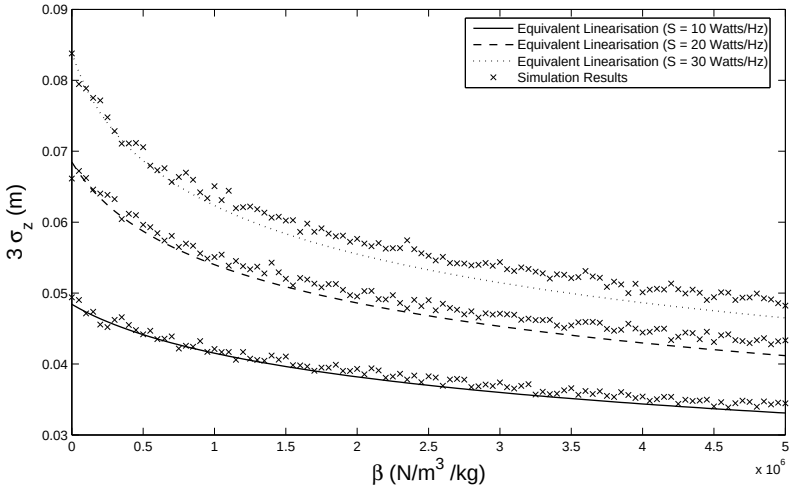

Figure 3: Comparison of $3\sigma_z$ as β is varied where $\omega_n = 40$ rad/s , $m = 0.02$ kg, $\theta = 0.12$ Ns/m. Solid and dashed lines represent results according to equivalent linearisation where $S = 10$ and 30 Watts/Hz respectively while crosses and dots represent results according to Monte-Carlo simulations where $S = 10$ and 30 Watts/Hz respectively.

5. Electrical Optimisation

As shown in equation (9), the power through the load resistor is proportional to the square of the relative velocity of the centre magnet. From equation (14), the expected value of relative velocity squared can be found:

$$E[z_2^2] = \int_{-\infty}^{\infty} z_2^2 A_2^{-1} e^{-\frac{z_2^2(4\zeta\omega_n + 2\gamma/m)}{S}} dz_2 = \frac{S}{2(4\zeta\omega_n + 2\gamma/m)}. \tag{31}$$

Substituting into equation (9), the expected power across the load resistor can be written as:

$$E[P_{load}] = \frac{SR_L\alpha^2}{2(4\zeta\omega_n + 2\gamma/m)(R_L + R_C)^2}. \tag{32}$$

With the aim of finding the optimum value of load resistance, equation (32) is differentiated with respect to R_L and set to zero. By saying that:

$$E[P_{load}] = \frac{f(R_L)}{g(R_L)} = 0, \tag{33}$$

then, using the quotient rule:

$$\frac{dE[P_{load}]}{dR_L} = g(R_L)\frac{df(R_L)}{dR_L} - f(R_L)\frac{dg(R_L)}{dR_L}. \tag{34}$$

By assigning

$$f(R_L) = SR_L\alpha^2, \tag{35}$$

and

$$g(R_L) = 2(4\zeta\omega_n + 2\gamma/m)(R_L + R_C)^2, \tag{36}$$

one finds that:

$$\begin{aligned}\frac{dE[P_{load}]}{dR_L} = &\left(8\zeta\omega_n(R_L + R_C)^2 + \frac{4(R_L + R_C)^2}{m}\right) S\alpha^2 \\ &- \left(16\zeta\omega_n(R_L + R_C) + \frac{4\alpha^2}{m}\right) SR_L\alpha^2 = 0.\end{aligned} \tag{37}$$

After manipulation, the optimum load resistance ($R_{L(opt)}$) can be expressed as a quadratic:

$$(-2\zeta\omega_n m)R_{L(opt)}^2 + (2\zeta\omega_n m R_C^2 + \alpha^2 R_C) = 0, \tag{38}$$

whose solution is easily obtained with the formula:

$$R_{L(opt)} = \pm\frac{\sqrt{(2\zeta\omega_n R_C m)^2 + 2\zeta\omega_n R_C m\alpha^2}}{2\zeta\omega_n m}, \tag{39}$$

where the (unfeasible) negative values of load resistance are neglected. Upon studying equation (39) one can see that, if $\alpha = 0$ then the optimum amount of power will be extracted when $R_L = R_C$. This is expected as it follows the fundamental principle of impedance matching [17]. However, when $\alpha \neq 0$ then the optimum load resistance is not equal to the coil resistance - this is illustrated by Figure 4.

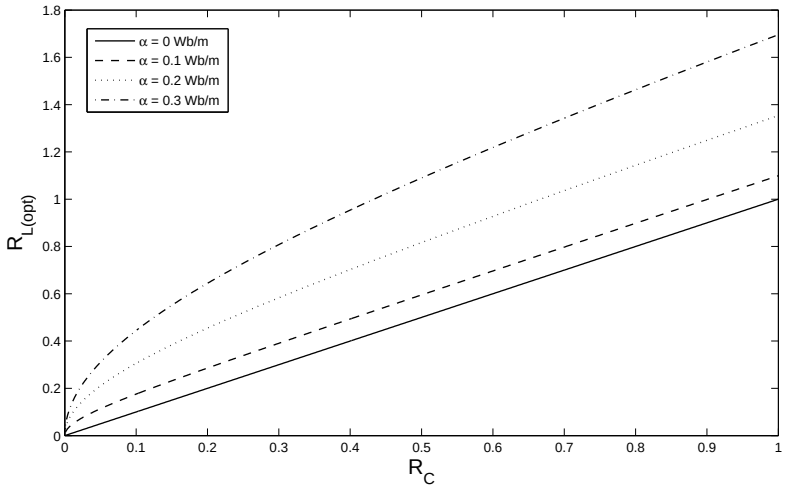

Figure 4: Variation of optimum load resistance with coil resistance for different values of α with $m = 0.02458$, $k = 56.2$, $k_3 = 86579$ and $c = 0.048$

Physically, this means that if the variation of magnetic flux with relative displacement is large then it will increase the value of optimum load resistance required. This may prove beneficial in situations where it is difficult to achieve a load resistance low enough to match that of the coil.

5.1. Experimental Validation

The purpose of this section was to experimentally verify the findings shown in Section 5 as well as some of the assumptions that were used in the modelling procedure shown in Section 2.

To begin with, the mechanical parameters of the system were identified using the apparatus shown in Figure 5(a) (a similar procedure is detailed in [16]). The device was attached to an electromagnetic shaker via an aluminium extension piece while the centre magnet was allowed to run along an aluminium rod via two sets of linear bearings. A Linear Variable Differential Transducer (LVDT) was used to measure the displacement of the shaker table. This signal was then fed through a Proportional Integral Differential (PID) controller to allow control of the shaker table displacement.

Using the controller, the shaker was excited with a displacement signal that resulted in a white noise acceleration with a flat power spectral density between 4 and 20 Hz, as shown in Figure 6. As the device had a natural frequency of approximately 8Hz, it was thought that the bandwidth of the acceleration spectrum was sufficiently large to capture the dynamics of the system. During each test, the displacement of the centre magnet was recorded using the laser.

During testing it became apparent that, to accurately model the dynamics of the device, the effects of friction would have to be included. This was achieved using Coulomb damping such that the equation of motion

became:

$$m\ddot{z} + c\dot{z} + kz + k_3 z^3 + F_d sgn(\dot{z}) = -m\ddot{y}, \tag{40}$$

where F_d represents the magnitude of the Coulomb damping force.

Using the shaker table time histories the model was excited with the same displacement time history that had been used experimentally and the resulting centre magnet displacements were compared with that of the experiment. A Self-Adaptive Differential Evolution Algorithm (SADE) (as described in [23]) was then used to find the mechanical parameters that led to the best match between the model and experimental time histories. The identified parameter values are shown in Table 1.

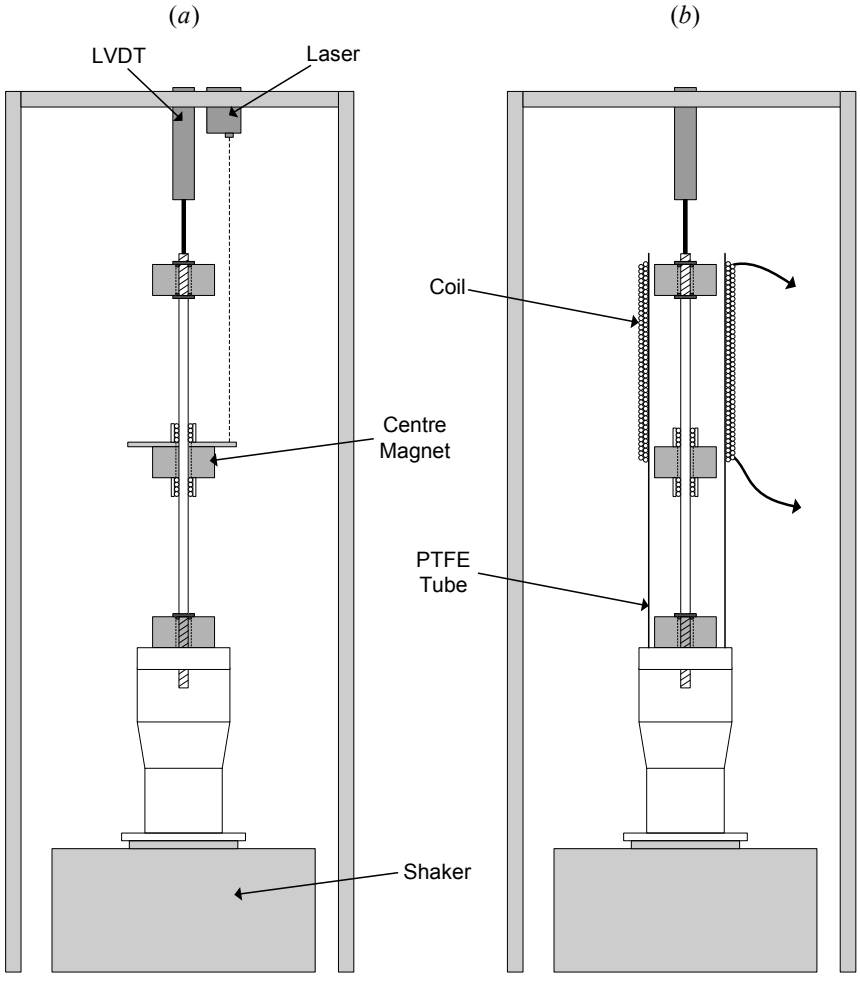

Figure 5: Schematic of experimental apparatus used to validate the (a) mechanical and (b) electrical parameters of the device.

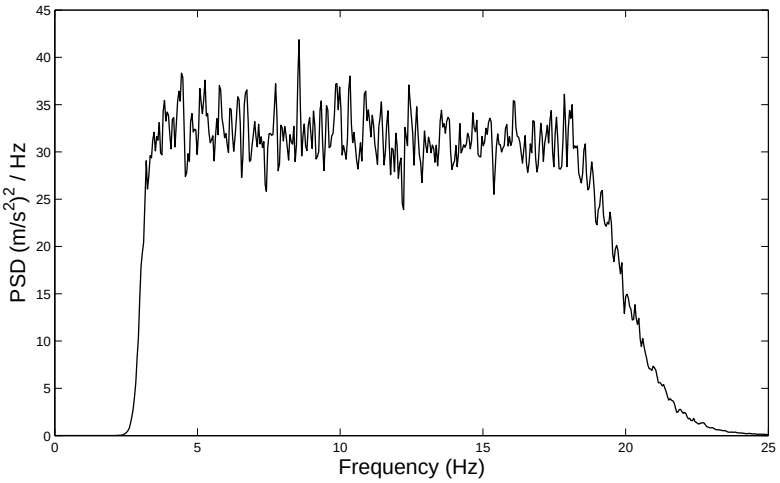

Figure 6: Example of base acceleration power spectral density.

Parameter	Value	Units
m	0.02358	kg
c	0.08863	Ns/m
F_d	0.02488	N
k	60.034	N/m
k_3	70565	N/m^3

Table 1: Parameters identified using the SADE algorithm.

Once the mechanical parameters of the device were identified, 83 turns of 0.5 mm diameter copper coil were wrapped around a PTFE tube which was subsequently attached to the shaker base - as shown in Figure 5(b). The output from the coil was then fed through a load resistor. The resistance of the coil was found to be 0.48 Ohms and the inductance was found to be negligible (verifying the assumption made in Section 2).

The relationship between the magnetic flux and the relative displacement of the centre magnet for a single turn of coil was found using the finite element package FEMM. Following an assumption made in Section 2, a linear approximation of the flux-displacement relationship was made. Figure 7 shows that the approximation was chosen under the assumption that only relatively small centre magnet displacements would take place. From the finite element simulations it was found that $\alpha_1 = 0.0024$ Wb/m (where α_1 represents the flux displacement relationship for one turn of coil). Multiplying by the number of turns on the device it was found that $\alpha = 0.1992$ Wb/m.

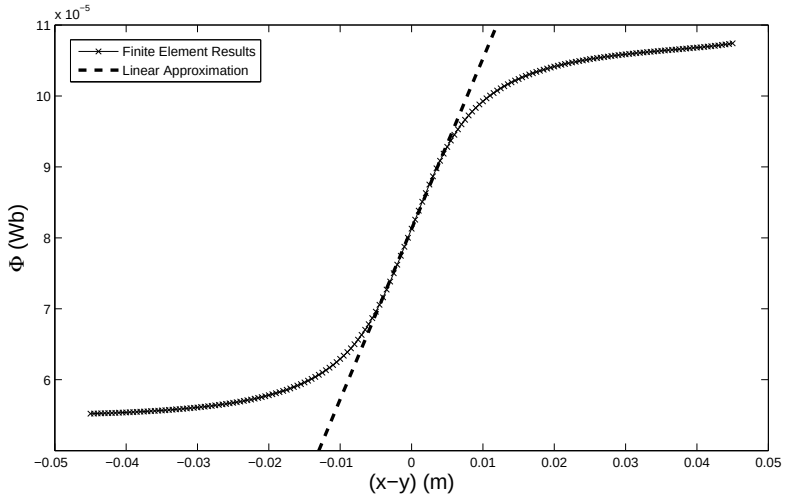

Figure 7: Finite Element simulation of flux displacement relationship. Dashed and solid lines represent simulation results and the linear approximation respectively.

The voltage across the load resistor of the device was compared with that of the model for different intensities of white noise base excitation - the results of which can be seen in Figures 8, 9, 10 and 11. For all of these tests a load resistance of 3 Ohms was used.

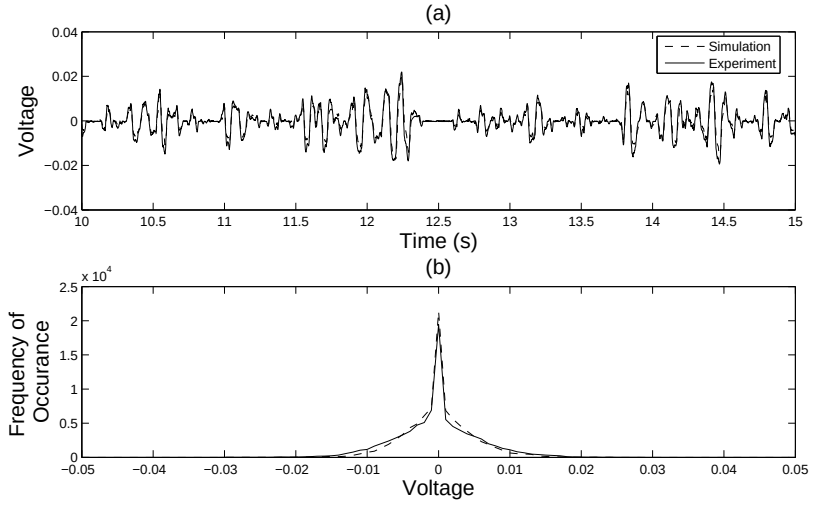

Figure 8: Comparison of voltage (a) time history and (b) histogram with an RMS base acceleration of 1.9 m/s^2. Dashed and solid lines represent the simulation and experimental results respectively.

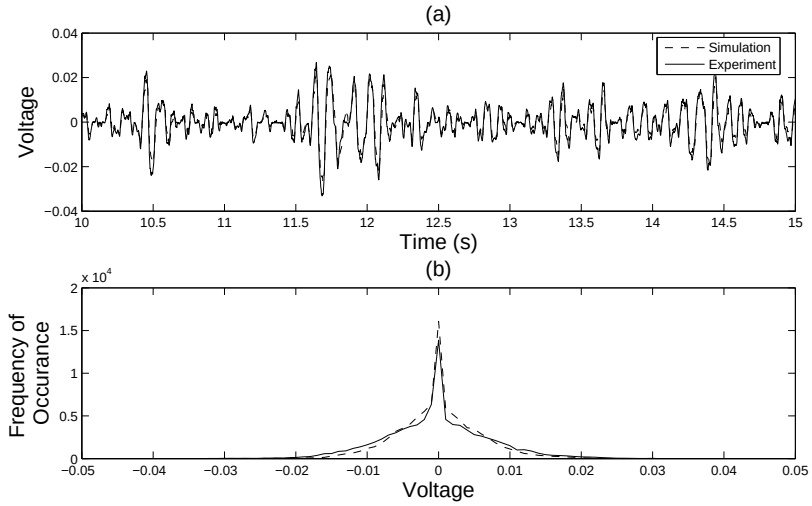

Figure 9: Comparison of voltage (a) time history and (b) histogram with an RMS base acceleration of 2.0 m/s^2. Dashed and solid lines represent the simulation and experimental results respectively.

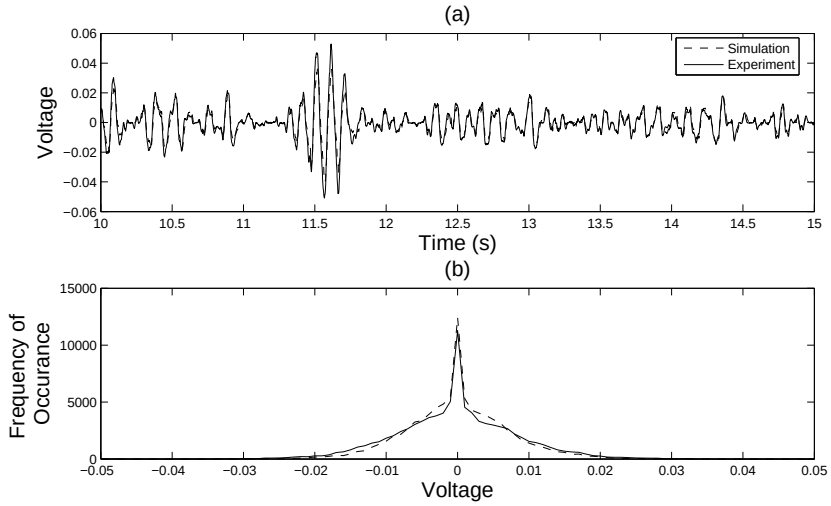

Figure 10: Comparison of voltage (a) time history and (b) histogram with an RMS base acceleration of 2.2 m/s^2. Dashed and solid lines represent the simulation and experimental results respectively.

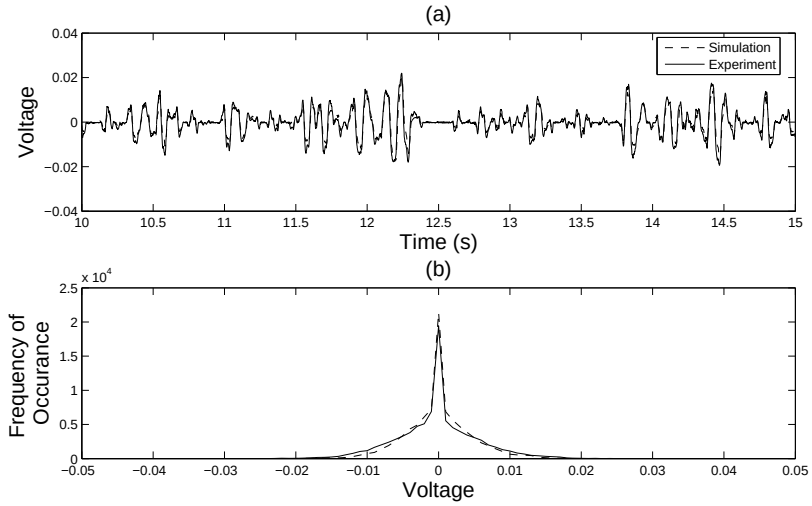

Figure 11: Comparison of voltage (a) time history and (b) histogram with an RMS base acceleration of 2.3 m/s^2. Dashed and solid lines represent the simulation and experimental results respectively.

It can be seen that the voltage output of the model has matched the experiment well for all conditions, thus validating the assumption that the inductance can be ignored and that the flux displacement relationship can be approximated as linear. Upon studying the results it can be seen that large peaks appear at the centre of all the histograms. This can be attributed to the centre magnet being held stationary by friction forces and, as a result, not inducing a voltage in the coil. This is confirmed by the fact that if friction is neglected in the model then the peaks disappear and smoother histograms are created.

The performance of the model was then compared with the experiment for different values of load resistance. With a coil resistance of 0.48 Ohms, the optimum load resistance predicted by equation (39) was found to be 0.67 Ohms. As a result, it was necessary to vary the load resistance by as little as 0.1 Ohms between tests - this was achieved using combinations of discrete resistors, each with a resistance of 0.1 Ohms. For larger changes in resistance a decade box was found to be sufficiently accurate.

Figure 12 shows how the expected power output of the device compared with two different simulations - one including and one neglecting the effects of friction. It can be seen that when friction is included, the simulation matches the experiment and that the optimum load resistance in both simulations as well as the experimental test was larger than that of the coil resistance. This is in keeping with the findings of the previous section.

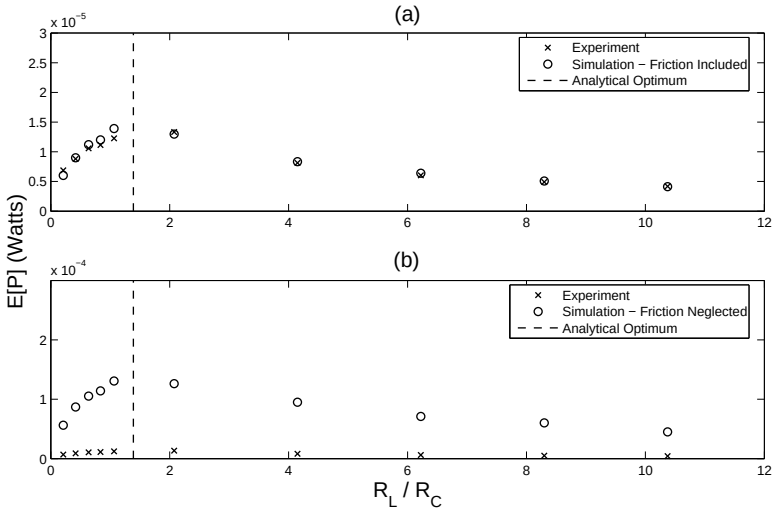

Figure 12: Expected power output for different values of load resistance where crosses represent experimentally identified values, dots and circles represent simulation results and the dashed lines represent the analytical optimum load resistance. Plots (a) and (b) represent simulation results where $F_d = 0.025$ and $F_d = 0$ Newtons respectively.

6. Discussion and Future Work

During the modelling procedure several assumptions were made and, although successfully validated experimentally, they are still worthy of some discussion.

Firstly, it was assumed that the flux displacement relationship could be approximated well as being linear. While adequate in this case, this assumption may not always be true. For example, if one were to excite the device sinusoidally at resonance then, as a consequence of the increased magnet displacements, the assumption that the flux displacement relationship is linear may weaken. This may actually lead to significant levels of nonlinear damping being introduced into the system (the magnitude of this effect would depend on whether the damping introduced by the coupling was significant when compared to the parasitic damping present in the device).

Secondly, it was assumed that the effects of inductance were negligible. As it is well known that a series combination of resistor and inductor acts as a low-pass filter then one would expect the importance of inductance to increase as the frequency of excitation increases. Typically, for low frequency signal filtering applications, inductances of several hundred henries are required - this is usually obtained by winding hundreds of turns of coil around a ferromagnetic material [24]. When measured, the inductance of the coil used in this work was found to be 4×10^{-8} henries - a value so small that one can safely assume that its effect can be considered negligible, especially when the majority of energy sources being considered for use with energy harvesters are of a relatively low frequency (bridge motion for example). However, although negligible in this case, the authors recognise that it may not be possible to apply this assumption universally to all electromagnetic energy harvesters. Recently, an analytical analysis in [25] showed that when the electrical time constant of

an energy harvesting device is close to its mechanical time constant, Duffing type nonlinearities can have a detrimental effect on its performance.

With regards to the dynamics of the device it is interesting to note that, to accurately model the experimental results, the Coulomb damping model had to be introduced to model the effects of friction. Attempts to include Coulomb damping in a FPK analysis of the system have proved difficult due to the presence of the Signum function and, as a result, an exact solution which dictates the effect of friction on the PDFs of the system could not be obtained. Although examples of the FPK equation being applied to systems with nonlinear damping can be found in the literature ([20][26] for example) the authors are unaware of an exact solution for a Coulomb damped oscillator.

The main assumption made in this work is that ambient vibrations can be modelled as broadband white noise signals. In practice the excitation would depend entirely upon the chosen environment for the device. Although broadband excitations may be considered more accurate than assuming a sinusoidal excitation, future work could be directed towards the response of devices to colored noise signals or signals with time varying dominant frequencies. It may also be interesting to investigate what effect tuning the load resistance to it's optimum value can have on the displacement variance of the device.

Finally, it is worth emphasising that this work is focused on the analysis of a mono-stable energy harvesting device. In [27] it was suggested that spring nonlinearities can be used to create a device which was bi-stable and that, if one were to excite the device such that it was jumping between the two energy wells, one would achieve superior broadband performance when compared to that of a linear device. An analytical analysis of the response of such a device to broadband random excitations using the FPK equation can be found in [10].

7. Conclusions

In this work, the response of a mono-stable nonlinear electromagnetic energy harvesting device to broadband white noise base accelerations was analysed. Firstly, using the FPK equation to find the stationary joint probability density of the system, it was shown that the introduction of cubic stiffness nonlinearities can help reduce the size of the device without effecting its power output. The method of Equivalent Linearisation was then used to verify this result. Secondly, the FPK equation was used to analyse the ability of the device to deliver power across a load resistor. Contrary to the principle of impedance matching, it was found that the optimum load resistance was not equal to that of the coil resistance. Experimental tests were then used to show that, although the effects of friction had been ignored in the modelling process, the optimum load resistance was indeed different to that of the coil resistance.

Appendix A. Solution of FPK Equation

For the sake of clarity, from now on $\eta = 2\omega_n\zeta + \gamma/m$. Assuming that the displacement and velocity displacement probability densities are independent then:

$$p = p_1(z_1) \times p_2(z_2). \tag{A.1}$$

Writing $p_1(z_1)$ and $p_2(z_2)$ as p_1 and p_2 respectively then, after some manipulation:

$$0 = \left[-\frac{z_2}{p_1}\frac{\partial p_1}{\partial z_1} + \frac{1}{p_2}\frac{\partial p_2}{\partial z_2}(\omega_n^2 z_1 + \beta z_1^3)\right] + \left[\eta + \eta\frac{z_2}{p_2}\frac{\partial p_2}{\partial z_2} + \frac{S}{4p_2}\frac{\partial^2 p_2}{\partial z_2^2}\right]. \tag{A.2}$$

As observed in [28], p is a solution of equation (A.2) if it satisfies:

$$\left[-\frac{z_2}{p_1}\frac{\partial p_1}{\partial z_1} + \frac{1}{p_2}\frac{\partial p_2}{\partial z_2}(\omega_n^2 z_1 + \beta z_1^3)\right] = 0, \tag{A.3}$$

$$\left[\eta + \eta\frac{z_2}{p_2}\frac{\partial p_2}{\partial z_2} + \frac{S}{4p_2}\frac{\partial^2 p_2}{\partial z_2^2}\right] = 0. \tag{A.4}$$

Using the product rule, equation (A.4) can be written as:

$$\frac{d}{dz_2}\left(\eta p_2 z_2 + \frac{S}{4}\frac{dp_2}{dz_2}\right) = 0. \tag{A.5}$$

Integrating with respect to z_2:

$$\eta p_2 z_2 + \frac{S}{4}\frac{dp_2}{dz_2} = C, \tag{A.6}$$

where C is a constant. Knowing that p_2 is a probability density function then, as z_2 approaches infinity, p_2 and all of its derivatives will approach zero therefore C must be equal to zero:

$$\eta p_2 z_2 + \frac{S}{4}\frac{dp_2}{dz_2} = 0. \tag{A.7}$$

After some manipulation and integrating with respect to z_2 one finds that:

$$p_2 = A_2 e^{-\frac{2\eta z_2^2}{S}}, \tag{A.8}$$

where, to satisfy the condition that

$$\int_{-\infty}^{\infty} p_2 dz_2 = 1, \tag{A.9}$$

then:

$$A_2^{-1} = \int_{-\infty}^{\infty} e^{-\frac{2\eta z_2^2}{S}} dz_2. \tag{A.10}$$

Once p_2 is known it can be substituted back into equation (A.3) so that, after some manipulation:

$$\frac{1}{p_1}\frac{dp_1}{dz_1} = -\frac{4\eta}{S}(\omega_n^2 z_1 + \beta z_1^3). \tag{A.11}$$

Integrating with respect to z_1 one finds that:

$$p_1 = A_1 e^{-\frac{4\eta}{S}\left(\frac{\omega_n^2}{2} z_1^2 + \beta z_1^4\right)}, \tag{A.12}$$

where, again, to satisfy the normalisation condition:

$$A_1^{-1} = \int_{-\infty}^{\infty} e^{-\frac{4\eta}{S}\left(\frac{\omega_n^2}{2} z_1^2 + \beta z_1^4\right)} dz_1. \tag{A.13}$$

As a result, the stationary probability density function of the system is:

$$p = A_1 e^{-\frac{4(2\omega_n\zeta+\gamma/m)}{S}\left(\frac{\omega_n^2}{2} z_1^2 + \beta z_1^4\right)} \times A_2 e^{-\frac{2(2\omega_n\zeta+\gamma/m)z_2^2}{S}}. \tag{A.14}$$

[1] S. P. Beeby, M. J. Tudor, and N. M. White. Energy harvesting vibration sources for microsystems applications. *Measurement Science and Technology*, 17(12):R175, 2006.

[2] C. B. Williams and R. B. Yates. Analysis of a micro-electric generator for microsystems. *Sensors and Actuators A: Physical*, 52(1-3):8 – 11, 1996. Proceedings of the 8th International Conference on Solid-State Sensors and Actuators Eurosensors IX.

[3] C.R. Saha, T. O'Donnell, H. Loder, S. Beeby, and J. Tudor. Optimization of an electromagnetic energy harvesting device. *IEEE Transactions on Magnetics*, 42(10):3509–3511, 2006.

[4] N.G. Stephen. On energy harvesting from ambient vibration. *Journal of Sound and Vibration*, 293(1-2):409 – 425, 2006.

[5] PD Mitcheson, TC Green, EM Yeatman, and AS Holmes. Architectures for vibration-driven micropower generators. *Journal of Microelectromechanical Systems*, 13(3):429–440, JUN 2004.

[6] B. P. Mann and N. D. Sims. On the performance and resonant frequency of electromagnetic induction energy harvesters. *Journal of Sound and Vibration*, 329(9):1348–1361, APR 26 2010.

[7] L. Gammaitoni, I. Neri, and H. Vocca. Nonlinear oscillators for vibration energy harvesting. *Applied Physics Letters*, 94(16), 2009. cited By (since 1996) 27.

[8] S. Adhikari, M.I. Friswell, and D.J. Inman. Piezoelectric energy harvesting from broadband random vibrations. *Smart Materials and Structures*, 18(11), 2009. cited By (since 1996) 27.

[9] Mohammed F. Daqaq. Response of uni-modal duffing-type harvesters to random forced excitations. *Journal of Sound and Vibration*, 329(18):3621–3631, AUG 30 2010.

[10] Mohammed F. Daqaq. Transduction of a bistable inductive generator driven by white and exponentially correlated gaussian noise. *Journal of Sound and Vibration*, 330(11):2554 – 2564, 2011.

[11] D.A.W. Barton, S.G. Burrow, and L.R. Clare. Energy harvesting from vibrations with a nonlinear oscillator. *Proceedings of the ASME International Design Engineering Technical Conferences and Computers and Information in Engineering Conference 2009, DETC2009*, 1(PART A):427–436, 2010. cited By (since 1996) 0.

[12] S. Beeby and N. White. *Energy Harvesting for Autonomous Systems*. Smart Materials, Structures, and Systems. Artech House, 2010.

[13] Dibin Zhu, Michael J. Tudor, and Stephen P. Beeby. Strategies for increasing the operating frequency range of vibration energy harvesters: a review. *Measurement Science & Technology*, 21(2), FEB 2010.

[14] L. Tang, Y. Yang, and C.K. Soh. Toward broadband vibration-based energy harvesting. *Journal of Intelligent Material Systems and Structures*, 21(18):1867–1897, 2010.

[15] B. P. Mann and N. D. Sims. Energy harvesting from the nonlinear oscillations of magnetic levitation. *Journal of Sound and Vibration*, 319(1-2):515–530, JAN 9 2009.

[16] P L Green, K Worden, K Atallah, and N D Sims. The effect of duffing-type nonlinearities and coulomb damping on the response of an energy harvester to random excitations. *Proceedings of EuroMech Colloquium 530, Structural Control and Energy Harvesting, University of Bristol*, 2011.

[17] R.H. Good. *Classical electromagnetism*. Number v. 1 in Saunders golden sunburst series. Saunders College Pub., 1999.

[18] A.T. Fuller. Analysis of nonlinear stochastic systems by means of the fokker-planck equation. *International Journal of Control*, 9(6), 1969.

[19] T.K. Caughey. Derivation and application of the fokker-planck equation to discrete nonlinear dynamic systems subjected to white random excitation. *Journal of the Acoustical Society of America*, 35(11), 1963.

[20] C.W.S. To. *Nonlinear random vibration: analytical techniques and applications*. Advances in Mechanical Engineering Series. Swets & Zeitlinger Publishers, 2000.

[21] M. Abramowitz and I.A. Stegun. *Handbook of mathematical functions with formulas, graphs, and mathematical tables*. Number v. 55, no. 1972 in Applied mathematics series. U.S. Govt. Print. Off., 1964.

[22] K. Worden and G.R. Tomlinson. *Nonlinearity in structural dynamics: detection, identification, and modelling*. Institute of Physics Pub., 2001.

[23] K. Worden and G. Manson. On the identification of hysteretic systems. part i: Fitness landscapes and evolutionary identification. *Mechanical Systems and Signal Processing*, (0):–, 2012.

[24] J.J. Brophy. *Basic electronics for scientists*. Schaum's Outline Series in Electronic & Electrical Engineering. McGraw-Hill, 1989.

[25] Mohammed F. Daqaq. On intentional introduction of stiffness nonlinearities for energy harvesting under white gaussian excitations. *Nonlinear Dynamics*, pages 1–17, 2012. 10.1007/s11071-012-0327-0.

[26] Y.K. Lin and G.Q. Cai. *Probabilistic structural dynamics: advanced theory and applications*. McGraw-Hill, 1995.

[27] F. Cottone, H. Vocca, and L. Gammaitoni. Nonlinear energy harvesting. *Physical Review Letters*, 102(8), 2009. cited By (since 1996) 78.

[28] T.K. Caughey and F. Ma. The exact steady-state solution of a class of non-linear stochastic systems. *International Journal of Non-Linear Mechanics*, 17(3):137–142, 1982.